

pubs.acs.org/cm Article

Salicylhydroxamic Acid as a Novel Switchable Adhesive Molecule

Kan Wang, Lokanath Patra, Bo Liu, Zhongtian Zhang, Ravindra Pandey, and Bruce P. Lee*



Cite This: Chem. Mater. 2023, 35, 5322-5330



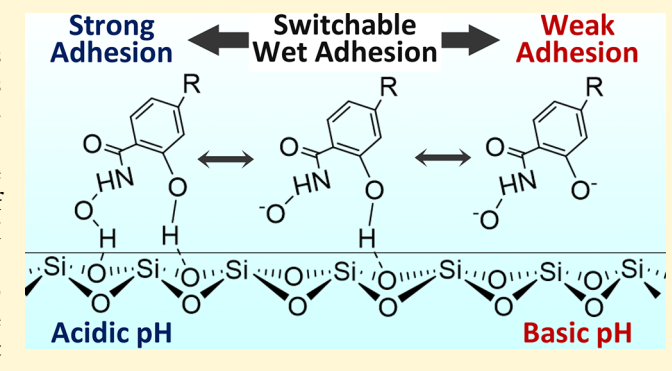
ACCESS I

III Metrics & More

Article Recommendations

Supporting Information

ABSTRACT: The feasibility of salicylhydroxamic acid (SHAM) to function as a pH-responsive, switchable adhesive molecule is explored here. Using a custom-built Johnson–Kendall–Roberts contact mechanics test setup, SHAM-containing adhesive demonstrated strong, wet adhesion to various surfaces (glass, titanium, polystyrene and amine-functionalized glass) at pH 5 with adhesive properties that were comparable to those of catechol. The work of adhesion of SHAM decreased by nearly 98% with increasing pH and fully recovered when treated with pH 5. Most impressively, SHAM recovered its adhesive property even after its exposure to pH as high as 11, indicating superior stability toward base treatment. This result contrasts the case of catechol, which did not recover its initial adhesive property due to irreversible oxidation.



Finally, density functional theory calculations were used to confirm that the observed tunable adhesion property was due to the deprotonation of SHAM.

1. INTRODUCTION

Smart adhesives demonstrate switchable adhesion properties in response to externally applied stimuli such as temperature, pH, light, and applied electricity. ^{1–3} Such ability to switch adhesion on demand has a wide range of potential applications in industrial assembly, advanced healthcare, and robotic manipulation. ^{4–8} However, existing switchable adhesives have limitations that include weakened underwater adhesion, adhesion to only a specific type of surface, requirement of extreme conditions to detach from a surface, or limited reversibility. ^{9–12} This paper aims to evaluate a novel, switchable adhesive molecule that could bind to various surfaces under wet conditions.

Mussels attach to various wet surfaces (e.g., rock, wood, and metal) using adhesive mussel foot proteins (MFPs).¹³ The main amino acid in MFPs responsible for underwater adhesion is 3,4-dihydroxyphenylalanine (DOPA), which contains a catechol-side chain.¹⁴ Catechol exhibits tunable adhesive properties depending on its oxidation state and has emerged as an adhesive molecule for designing moisture-resistant smart adhesives that are responsive to pH and applied electricity. 15,16 Catechol forms reversible non-covalent bonds such as hydrogel bonding, $\pi - \pi$ interaction, cation $-\pi$ interaction, and metal ion coordination in its reduced state. 17 Upon oxidation, catechol is transformed into the poorly adhesive quinone form. However, quinone is highly reactive and undergoes irreversible crosslinking, which greatly limits its reversibility. 18-21 While it is possible to protect catechol using boronic acid, it is sometimes difficult to fully dissociate the catechol-boronate complex to fully recover the initial adhesive property of catechol. 22,23 Therefore, there is a need to find a novel, reversible, and switchable adhesive molecule that does not undergo autoxidation.

Salicylhydroxamic acid (SHAM) consists of a benzene ring with pendant hydroxamic acid and hydroxyl group (Figure 1a). SHAM is widely used in antitubercular medications and antiaging and skin conditioning cosmetic products. ^{24–26} Given the structural similarity between SHAM and catechol, we hypothesize that SHAM can potentially function as an adhesive molecule with the ability to form interfacial bonds through hydrogen bonding, π – π interaction and cation– π interaction. SHAM is also a known chelator of metal ions, ²⁷ which can potentially facilitate its binding to a metal surface. Additionally, SHAM deprotonates and protonates in response to pH without oxidation (pK_{a1} = 7.4 and pK_{a2} = 9.7). ^{28,29} Deprotonation of SHAM can potentially reduce its interfacial bonding capabilities (Figure 1b), making it suitable to function as a reversible, pH-responsive adhesive molecule.

In this study, we aimed to determine the feasibility of SHAM to function as a novel, switchable adhesive that responds to changing pH. To this end, we synthesized a methacrylated monomer containing SHAM, *N*,2-dihydroxy-4-methacrylamidobenzamide (DHMAAB) (Figure 1c), which was further

Received: March 3, 2023 Revised: June 28, 2023 Published: July 13, 2023





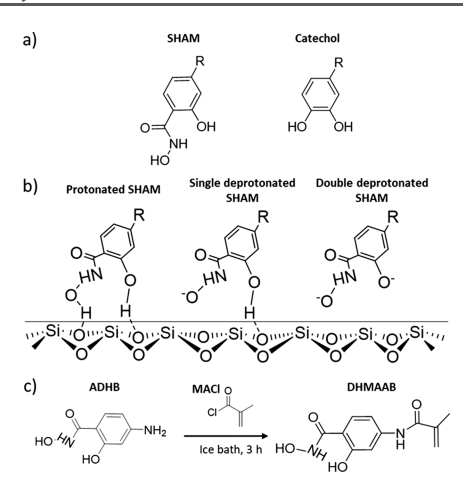


Figure 1. (a) Chemical structures of SHAM and catechol. (b) Proposed interfacial bonding of SHAM to the silica surface. With increasing pH (left to right), SHAM deprotonates and reduces its interfacial bonding capabilities. (c) Synthesis of SHAM-based monomer, DHMAAB, by reacting 4-amino-*N*,2-dihydroxybenzamide hydrochloride with methacryloyl chloride.

polymerized into an adhesive coating. We then evaluated the pH-dependent, switchable adhesive properties of SHAM on various contacting surfaces using Johnson—Kendall—Roberts (JKR) contact mechanics test. Additionally, density functional theory (DFT) simulation was utilized to analyze the molecular-level adhesion of SHAM to the silica surface. The adhesive property of SHAM was compared with that of catechol.

2. MATERIALS AND METHODS

2.1. Materials. 4-Amino-*N*,2-dihydroxybenzamide (ADHB) was purchased from EnamineStore. Ethanol, tetrahydrofuran (THF), ethyl acetate, phosphate-buffered saline (PBS), hydrochloric acid (HCl), sodium hydroxide (NaOH), sodium chloride (NaCl), hexane, dimethyl sulfoxide (DMSO), trichloro(1H,1H,2H,2Hperfluorooctyl)silane (97%), toluene, acetone, methoxyethyl methacrylate (MEA), triethylamine, 3-(trimethoxysilyl)propyl methacrylate (TMSPMA), mechacryloyl chloride (MACl), and (3-aminopropyl) trimethoxysilane (APTS) were purchased from Sigma-Aldrich (St. Louis, MO). 2,2-Dimethoxy-2-phenylacetophenone (DMPA) and methylene-bis-acrylamide (MBAA) were purchased from Acros Organics. Titanium (Ti) ball (1/4" diameter), polystyrene (PS) rod (3/8" diameter), and polytetrafluoroethylene (PTFE) (3/8" diameter) were purchased from McMaster-carr (Elmhurst, IL). PS rod was trimmed into 1/4" diameter hemispheres using an 8026 J Clausing/ Colchester Manual Engine Lathe (Clausing Industrial; Kalamazoo, MI). Borosilicate glass hemispheres (1/4" diameter) were purchased from ISP Optics (Orlando, FL). The amine-functionalized glass was prepared by treating borosilicate glass hemispheres with APTS following a published protocol.²¹ The acidic solutions (pH 3, pH 5) were prepared using deionized (DI) water, 0.1 M NaCl, and 1 M HCl. The buffers, including pH 7.4, pH 8, and pH 9, were prepared using deionized (DI) water, PBS, and NaOH. pH 11 solution was prepared using deionized (DI) water, 0.1 M NaCl, and NaOH. Dopamine methacrylamide (DMA) was synthesized according to a previously published protocol.³⁰

2.2. Monomers Synthesis and Characterization. DHMAAB was synthesized by reacting ADHB with MACl (Figure 1c). First, 2 mmol of ADHB dissolved in 10 mL of methanol. Then, 2 mmol of MACl in 2 mL of THF was slowly added to the ADHB solution, followed by 6 mmol of triethylamine. The mixture was stirred in a nitrogen atmosphere for 3 h in an ice bath. The resulting DHMAAB was extracted with ethyl acetate and further purified by column chromatography using ethyl acetate and hexane (2:1) as the mobile phase. DHMAAB was then crystallized under vacuum. 20 mg of

DHMAAB was dissolved in 0.5 mL of DMSO- d_6 for nuclear magnetic resonance (NMR) characterization using spectroscopy (Ascend 500 MHz, Bruker, MA). The absorption spectra of 0.1 mmol DHMAAB water solutions at different pH levels were examined using UV–vis spectroscopy (LAMBDA35, PerkinElmer, MA).

2.3. Preparation of Adhesive Coatings. Glass slides were first functionalized with a polymerizable methacrylate group, followed by in situ polymerization of adhesive monomers (Figure 2). The glass

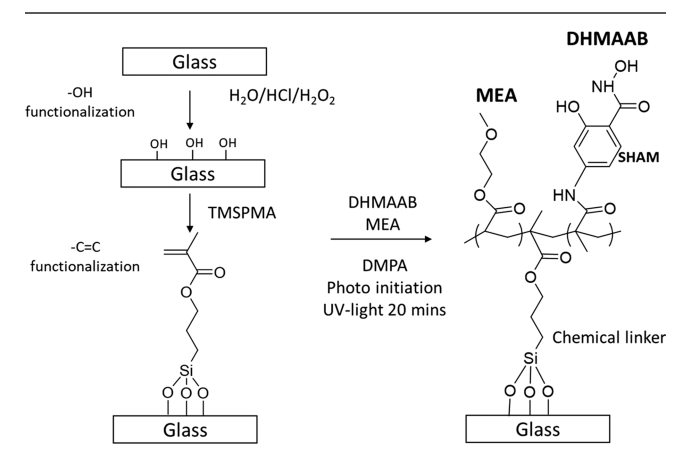


Figure 2. A schematic showing the coating process of chemically immobilizing thin adhesive coatings onto glass slides.

slides were immersed in a solution containing H₂O, HCl, and H₂O₂ with a volume ratio of 5:1:1 for 10 min, followed by rinsing with deionized (DI) water. Then, the glass slides were treated with a 3% v/ v TMSPMA solution in a DI water-ethanol mixture (volume ratio = 1:1) for 1 h. The samples were rinsed in DI water and dried with N₂. Adhesive coatings were chemically linked to the methacrylate group functionalized glass slides by free radical polymerization. To prepare SHAM-based coating, 1 M MEA with 10 mol % of DHMAAB and 0.2 mol % of DMPA were dissolved in 75% (v/v) DMSO and DI water. The precursor solution was degassed and purged with nitrogen gas three times. 15 μ L of the precursor solution was then applied to a TMSPMA-functionalized glass slide, which was further covered with a fluorinated cover glass and photoinitiated for 20 min in a UV crosslinking chamber (XL-1000, Spectronics Corporation; Westbury, NY) located in a nitrogen-filled glovebox (Plas-Labs; Lansing, MI). The fluorinated cover glass was prepared by submerging it in a mixture containing 1% v/v trichloro(1H,1H,2H,2H-perfluorooctyl)silane solution in toluene for 20 min, rinsing it in toluene, and then drying it in a chemical hood. The adhesive coating was purified by soaking it in DMSO, ethanol, and DI water for 5 min, 5 min, and overnight. The catechol-based precursor solution was prepared by dissolving 1 M MEA with 10 mol % of DMA, 1 mol % of MBAA, and 0.2 mol % of DMPA in 75% (v/v) DMSO and DI water. The catechol-based coating was prepared in the same method and washed with a solution of pH 5 overnight. The samples were freeze-dried and analyzed using attenuated total reflectance Fourier transform infrared (ATR-FTIR) spectroscopy technique (IRTracer-100, Shimadzu Corporation; Kyoto, Japan). The surface thickness was measured using a Filmetrics 3D Profilometer (Profilm3D, Filmetrics, Inc.; San Diego, CA) and reported as average thickness. The surface morphology was characterized using a field emission scanning electron microscope (FE-SEM; Hitachi S-4700, Hitachi, Ltd.; Tokyo, Japan).

2.4. JKR Contact Mechanics Tests. JKR contact mechanics device used in this study consisted of a custom-built indenter (ALS-06, Transducer Techniques), a 10-g load cell (Transducer Techniques), and a high-resolution miniature linear stage stepper motor (MFA-PPD, Newport) (Figure 3). The indenter was mounted with one of four types of hemispheres with a diameter of 1/4". The hemispheres consisted of borosilicate glass (Si), titanium (Ti), amine-functionalized borosilicate glass (NH₂), or polystyrene (PS). The hemisphere was brought into contact with the adhesive

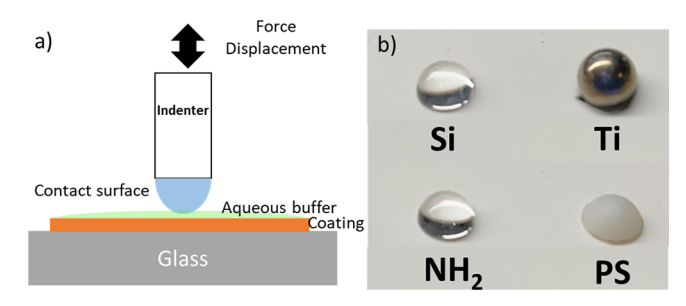


Figure 3. (a) Schematic of JKR contact mechanics test on a thin coating sample. (b) Photographs of silica (Si), titanium (Ti), aminefunctionalized silica (NH_2), and polystyrene (PS) hemispheres were used as contact surfaces.

coating at a speed of 1 μ m/s until a maximum preload of 10 mN and then retracted at the same speed. Prior to the contact, the interface was wetted with 40 μ L of interfacial solution buffered at a desired pH.

Based on a JKR theory, which describes a spherical tip onto a film on a rigid substrate, the adhesion energy equals to critical energy release rate (G_c) in a load-controlled experiment, the maximum tensile force (F_{max}) was used to determine the G_c as calculated by:

$$G_{\rm c} = \frac{2}{3\pi R} F_{\rm max} \tag{1}$$

where *R* is the radius of the hemispheric contacting surface.

Prior to adhesion testing, the adhesive coatings were first incubated at different pH levels for 1 h. To study the switchability of the adhesive coating, the coating was incubated at a given pH level for 1 h before the subsequent contact cycle. The pH of the incubation liquid and the interfacial solution was kept the same for a given contact cycle. To investigate the effect of indentor speed on the measured $G_{\rm c}$ values, tests were performed at 0.3, 0.5, and 1 μ m/s. To investigate the effect of capillary effect, the amount of the interfacial liquid was increased up to 300 μ L. For elevated liquid level, a well was created around the contact area using a rubber ring with a diameter of 10 mm to contain the extra liquid.

2.5. Density Functional Theory. The interaction energies of the adhesive molecules with the silica surface were calculated using density functional theory. The Vienna ab-initio simulation package (VASP) based on the projected augmented wave (PAW) pseudopotentials was employed. 36,37 The Perdew–Burke–Ernzerhof form of the generalized gradient approximation (PBE-GGA) was used with the cut-off energy of 500 eV.38 The energy and force convergence criteria were set to 1×10^{-5} eV and 0.01 eV/Å, respectively, and the Monkhorst-Pack k-point mesh of $5 \times 5 \times 1$ was used for calculations.³⁹ The hydroxylated silica surface from the (001) surface of α -cristobalite was used as the model surface. The surface was modeled with a $3 \times 3 \times 1$ supercell and a vacuum thickness of 20 Å. Different thicknesses of silica surfaces were tested to find the optimal surface thickness and six layers of Si were sufficient to describe the adsorption process of the considered catechol and SHAM molecules based on the calculated surface energy (Figure S1). The top Si layer was passivated with two -OH groups, generating geminal silanols (SiOH), while the bottom layer of Si atoms was terminated by H atoms. The optimized structural parameters of the Si surface match those from previous publications (Table S1).^{40,41}

To determine the optimum orientation for the adhesive molecule with respect to the surface, SHAM was oriented in both horizontal and vertical arrangements to determine the equilibrium configurations with the minimum energy (Figure S2). The distance between the molecule and the surface was varied in steps of 0.5 Å while keeping the atomic position fixed. The perpendicular-1 configuration of SHAM, where both the hydroxamic acid and hydroxyl group were pointing downward, had the lowest energy among the three configurations with an equilibrium distance of ~2.2 Å. This configuration was used in subsequent calculations. The configuration

was then fully relaxed by fixing the bottom two layers of the surface. The dispersion interaction has not been considered in our calculations, as the change in pH was reported to affect only the electrostatic interaction between the molecule and the surface. 42

To determine pH-dependent interaction strength between a surface (S) and a molecule (M), the interactions between all combinations of their neutral (S 0 and M 0) and deprotonated (S $^{-1}$, M $^{-1}$, and M $^{-2}$) states were determined. At a specific pH, the pH-dependent binding energy ($E_B^{\rm ph}$) is given by:⁴²

$$E_{\rm B}^{\rm pH} = \sum_{i=-1}^{0} \sum_{j=-2}^{0} E_{S^i M^j} F_{S^i} F_{M^j}$$
 (2)

where F is the fractional concentration and E is the interaction energy of the combinations. Fractional concentration of S and M was evaluated using modified Henderson–Hasselbalch equations: 42

$$F_0 ext{ (neutral)} = \frac{[H^+]^2}{[H^+]^{2+} + K_{al} \cdot [H^+] + K_{al} \cdot K_{a2}}$$
 (3)

$$F_{-1} \text{ (deprotonated)} = \frac{K_{al} \cdot [H^+]}{[H^+]^{2+} + K_{al} \cdot [H^+] + K_{al} \cdot K_{a2}}$$
(4)

$$F_{-2} \text{ (deprotonated)} = \frac{K_{a1}. K_{a2}}{[H^+]^{2^+} + K_{a1}. [H^+] + K_{a1}. K_{a2}}$$
(5)

where $K_{\rm a1}=10^{-{\rm p}K_{\rm a1}}$, $K_{\rm a2}=10^{-{\rm p}K_{\rm a2}}$, and $[{\rm H}^+]=10^{-{\rm p}{\rm H}}$. The p $K_{\rm a}$ values for silica vary from 4.5 to 8.5 depending on the surface's arrangement of the —SiOH groups. ^{43,44} Here, a p $K_{\rm a}$ value of 7.5 was utilized, which was the mid value of 4.5 and 8.5 estimated by the surface complexation model. ⁴⁵ The p $K_{\rm a}$ values of SHAM were 7.4 and 9.7 for the hydroxamic acid and phenol, resepectively. ²⁸ The p $K_{\rm a}$ value of 9.5 was used for catechol. ⁴⁶ The second p $K_{\rm a}$ value (11.5) for catechol was not utilized in our calculations is higher than the pH range that we are considering. Finally, the interaction energy ($E_{\rm int}$) of an adhesive molecule interacting with the silica surface was calculated as:

$$E_{\rm int} = E_{\rm silica+molecule} - E_{\rm silica} - E_{\rm molecule}$$
 (6)

2.6. Statistical Analysis. The R Project software was used to perform statistical analysis. One-way analysis of variance (one-way ANOVA) with the Tukey method and Student's t-test was used for comparing multiple and two groups, respectively, using a *p*-value of 0.05

3. RESULTS AND DISCUSSION

DHMAAB was synthesized in one step to obtain a polymerizable monomer with a SHAM side chain functionalized with methacrylamide (Figure 1c). The ¹H NMR spectra of DHMAAB confirmed the presence of the hydroxamic acid (9.90 and 7.76 ppm), phenolic hydroxyl (13.14 ppm), protons on the benzene ring (7.77, 7.35, and 7.16 ppm), as well as the methyl group (1.94 ppm) and a double bond (5.81 and 5.55 ppm) found in the methacrylamide (Figure S3). UV-vis spectra demonstrated the pH-dependent nature of the SHAM side chain (Figure S4). SHAM displayed the protonated form with a peak at λ_{max} of 304 nm at a pH between 3 and 5.²⁹ At intermediate pH levels of 7.4 and 9, the UV-vis spectra exhibited a decrease in the absorbance associated with the protonated SHAM ($\lambda_{max} = 304$ nm) and an increase in the absorbance at 336 nm associated with the formation of the single deprotonated form of SHAM. When the pH was increased beyond 9, a new peak was formed at 334 nm, corresponding to the peak of the double deprotonated form of SHAM.

The adhesive coatings were covalently linked to the surface of glass slides (Figures 2 and S5). The average thicknesses of

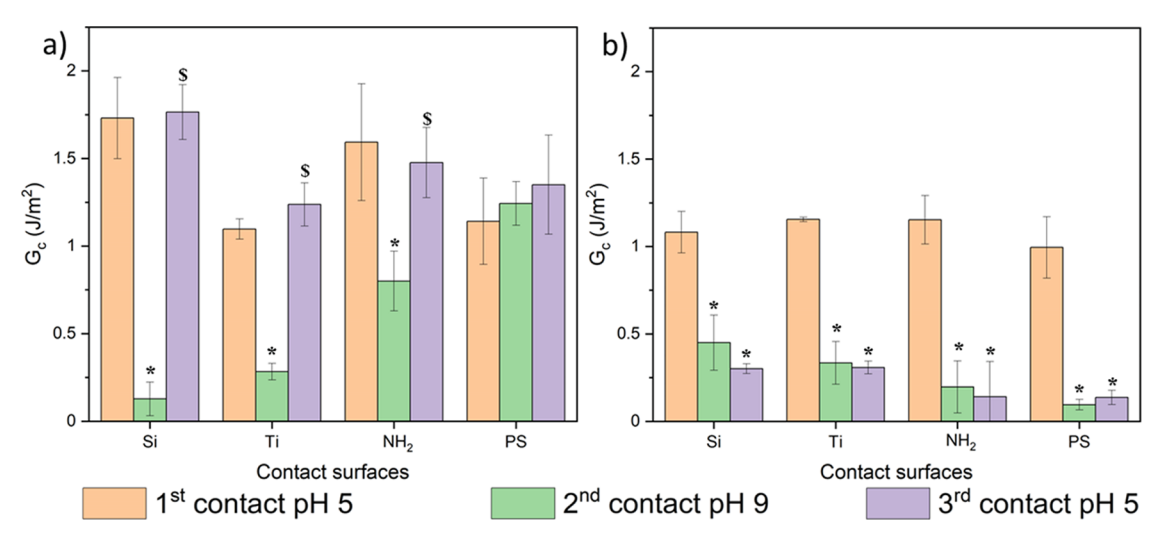


Figure 4. G_c of (a) SHAM-containing adhesive and (b) catechol-containing adhesive when contacting different surfaces including borosilicate glass (Si), titanium (Ti), amine-functionalized borosilicate glass (NH₂), and polystyrene (PS). Adhesive coatings were subjected to three repeated contact cycles tested sequentially at pH 5, 9, and then 5. *p < 0.05 when compared to the first contact at pH 5. *p < 0.05 for the third contact cycle when its value differs from that of the third contact at pH 9. (n = 3).

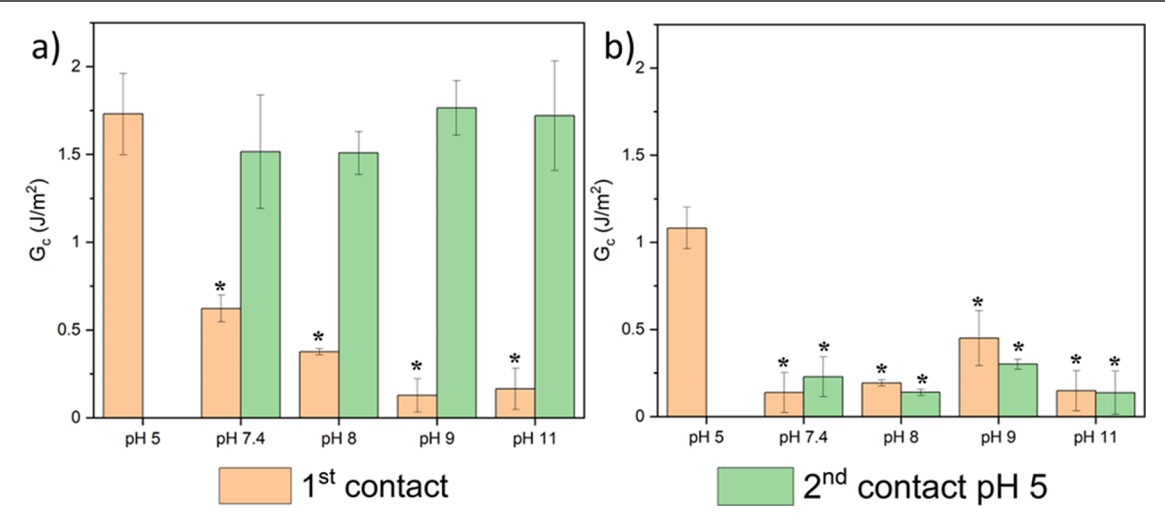


Figure 5. G_c of (a) SHAM-containing adhesive and (b) catechol-containing adhesive when contacting Si surface. The first contact was tested at different pH levels ranging from pH 5 to 11. The second contact was performed at pH 5. *p < 0.05 when compared to the first contact at pH 5. (n = 3).

SHAM-based and catechol-based coating were 1.35 \pm 0.10 and $1.61 \pm 0.33 \mu m$, respectively. The coating appeared homogeneous based on SEM images (Figure S6). The polymerizable methacrylate group was first covalently linked to the glass surface via silane chemistry using TMSPMA. An adhesive coating consisting of 10 mol % DHMAAB and MEA was polymerized and immobilized onto the slides through photoinitiated free radical polymerization. For comparison purposes, catechol-containing adhesive was prepared similarly using DMA instead of DHMAAB. The composition of the adhesive coating was verified using ATR-FTIR spectroscopy (Figure S7). FTIR spectra showed the presence of the MEA backbone (C=O at 1730 cm⁻¹), benzene ring (C=C at 1448 and 1521 cm⁻¹), and N-O stretching (hydroxamic acid) at 1597 cm⁻¹, which distinguished SHAM-containing adhesive from catechol-containing adhesive.

JKR contact mechanics test was chosen to investigate the interfacial bonding behavior of SHAM-containing adhesive when contacting four different surfaces: borosilicate glass (Si),

titanium (Ti), amine-functionalized borosilicate glass (NH₂), and polystyrene (PS) (Figure 3). The JKR test setup enabled us to investigate adhesion in the presence of an interfacial liquid with a specific pH, control the chemistry of the contacting surface, and minimize the contribution of the bulk mechanical property of the adhesive.¹⁷ The adhesive coatings were subjected to three repeated contact cycles tested sequentially at pH 5, 9 and then 5. pH 5 was chosen to evaluate the adhesive property of protonated SHAM and compare it to that of catechol in its reduced form. At pH 9, SHAM is converted to the deprotonated state, while catechol is oxidized. The third cycle evaluates the ability of the adhesive to recover its initial adhesive property. Exemplary contact curves and maximum tensile data are shown in Figures S8–S10 and S12–S15.

SHAM demonstrated strong adhesion at pH 5 and weak adhesion at pH 9 (Figure 4). Using Si as the example, the measured critical energy release rate (G_c) was 1.73 \pm 0.23 J/m² at pH 5. This value decreased by more than 94% when

tested at pH 9. When the SHAM-based coating was further incubated in a pH 5 buffer, it fully regained its initial adhesive properties $G_{\rm c}=1.76\pm0.17~{\rm J/m^2}$. This suggested that the protonated form of SHAM is responsible for elevated interfacial bonding and could be tuned by changing pH. Most importantly, the adhesive properties of SHAM are fully recoverable.

While SHAM demonstrated similar pH-responsive adhesive properties when contacting Ti and NH₂ surfaces, the initial $G_{\rm c}$ values at pH 5 were 37 and 8% less than that of the Si surface, respectively. This indicated that SHAM binds more strongly with Si. At pH 9, SHAM retained marginal levels of adhesion to the NH₂ surface ($G_{\rm c}$ = 0.80 ± 0.17 J/m²), potentially due to an increased positive charge on the surface for cation— π interaction. Interestingly, the adhesive properties of the SHAM-based coating on PS were independent of pH. This indicates that the interaction between SHAM and PS is based on π – π interaction and is not affected by the deprotonation of SHAM.

The measured adhesive properties for SHAM were mostly comparable to those measured for catechol. The interaction between SHAM and Si surface was approximately 1.5 times stronger than that of catechol. Similar to SHAM, catechol demonstrated decreased adhesion with increasing pH (Figure 4b). However, when further tested at an acidic pH in the 3rd contact cycle, catechol did not recover its initial adhesive property. This data corroborates previous findings where catechol irreversibly oxidizes after exposure to the basic condition.²² Notably, catechol oxidizes to form quinone, which forms a fully conjugated cyclic dione structure (Figure S11). As such, it lost its ability to interact with NH₂ and PS surfaces through cation $-\pi$ and π - π interactions, respectively. This differs from SHAM, which retained a higher level of adhesion at pH 9 compared to catechol. This indicated that SHAM retained its benzene ring structure and did not autoxidize.

The ability of SHAM to recover its adhesive property after treatment at different pH levels (pH 5–pH 11) was further evaluated using a Si surface (Figure 5). The adhesive properties of SHAM decreased with increasing pH levels, potentially due to the deprotonation of the pendant hydroxamic acid and hydroxyl group. However, regardless of the pH, SHAM fully recovered its initial adhesion strength when tested at pH 5 in the second contact cycle. Most notably, SHAM recovered its adhesive properties even after it was first incubated at pH 11, demonstrating its impressive stability to base treatment. Conversely, catechol lost its adhesive property when treated with a basic solution and did not regain its initial adhesive properties after subsequent incubation at pH 5.

To further investigate the adhesion switching capability of SHAM, a JKR contact mechanics test was performed on SHAM-based coating after repeatedly incubating in pH 5 and 9. Over five complete contact cycles, the adhesive properties of SHAM were repeatedly modulated with changing pH (Figure 6). The measured G_c values of SHAM-based coating were reduced by 83–88% after each treatment with basic pH. G_c recovered successfully to their initial level with the treatment of pH 5. These results indicated that the SHAM-based coating could repeatedly switch its adhesive properties in a pH-dependent manner.

To investigate the influence of the indentor speed on the measured G_c values, JKR contact mechanics tests were conducted on the SHAM-based coating at indentation and

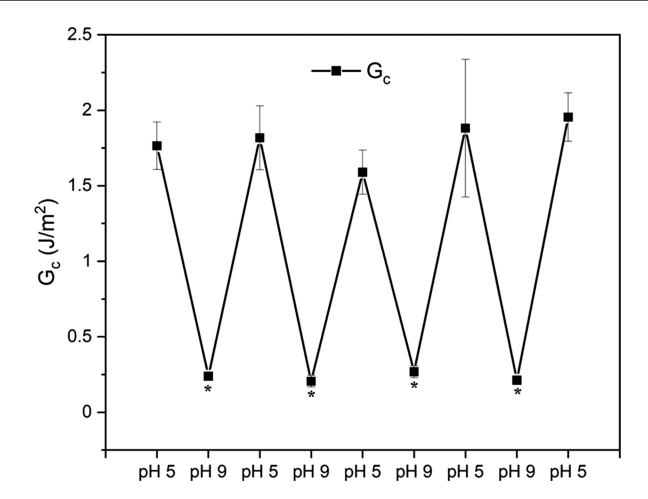


Figure 6. G_c of SHAM-containing adhesive was repeatedly tested in pH 5 and pH 9. *p < 0.05 when compared to the first contact at pH 5. (n = 3).

retraction speeds of 0.3, 0.5, and 1 μ m/s (Figure S16). The G_c values for 0.3 and 0.5 μ m/s were at a similar level but increased slightly when tested at 1 μ m/s. It is not clear if the increase in the G_c value was attributed to water being squeezed out at the interface during contact or if this is due to the viscoelastic property of the material itself. ^{47,48} However, given that all the experiments were performed in the same indentor speed and that all the coatings are composed mostly of the same composition, we expect that a similar level of increase in the G_c values would be measured in all of our experiments. Additionally, the measured changes in G_c values as a result of pH change were much greater than the differences observed as a result of changes in the indentor speed. Similarly, we investigated the effect of capillary effect on the measured G_c values by varying the amount of interfacial liquid (Figure S17). The G_c values were not statistically different regardless of the amount of interfacial liquid (Figure S18). This indicates that the capillary effect is not a factor in our adhesion testing. Additionally, we estimated the capillary force (0.894 mN from eq $\mathrm{S1})^{49}$ to be negligible when compared to the F_{max} values

To understand the interaction of SHAM with the Si surface, we performed DFT calculations using hydroxylated silica surface consisting of the (001) surface of α -cristobalite. Six Si layers were used to simulate the surface in the periodic slab model (Figure S1). The top Si layer was passivated with two –OH groups to generate geminal silanols (SiOH). The DFT results find that the equilibrium configuration consists of SHAM pointing perpendicularly toward the surface (Figure 7). We note that our DFT results are similar to those reported for the case of catechol interacting with the Si surface. For the subsequent analysis, we used the equilibrium configuration of SHAM interacting with the Si surface.

To evaluate the pH dependency of SHAM—Si interactions, DFT calculations were performed on the conjugated complexes of the surface (S) and the adhesive molecule (M), having six possible combinations of their neutral (S⁰ and M⁰) and deprotonated (S⁻¹, M⁻¹, and M⁻²) states (Figure S19). The calculated binding energy shows that all combinations except S⁰M⁻² and S⁻¹M⁻² are stable. For S⁰M⁰, the interaction was mediated by the hydrogen bonds formed between H atoms of the hydroxamic acid and phenol groups with silanol oxygen atoms of the surface with

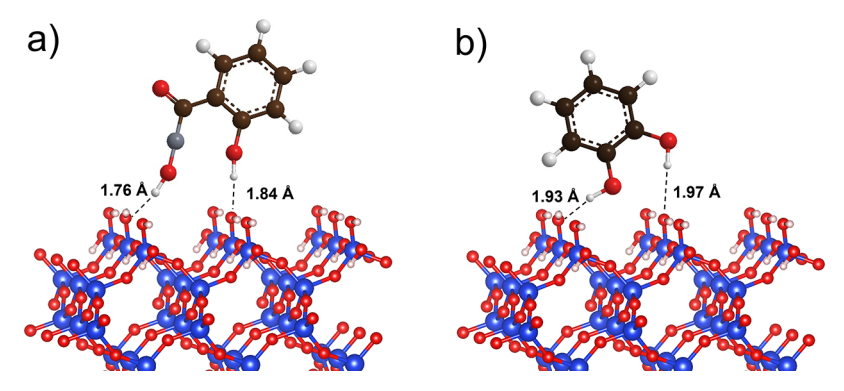


Figure 7. Equilibrium configurations of (a) SHAM and (b) catechol on the silica surface. The dashed lines indicate hydrogen bonds formed between the adhesive molecules and the Si surface.

interaction energy $(E_{\rm int})$ of -24.37 kcal/mol. Bader charge analysis showed that a charge transfer of \sim 0.1e was associated with this interaction. On the other hand, $S^{-1}M^0$ is highly stable with $E_{\rm int} = -42.4$ kcal/mol. This stability can be attributed to a charge transfer from the H atoms of the molecule to the deprotonated silica surface. We further note that the interactions within S^0M^{-1} and $S^{-1}M^{-1}$ were slightly attractive, with $E_{\rm B}$ of -10.0 and -5.4 kcal/mol, respectively. Similar to the salicylic acid interaction with silica reported in a previous study, 51 the interactions in these complexes were mediated by proton sharing between the O atom of the deprotonated SHAM and the H atom of the surface. Finally, S^0M^{-2} and $S^{-1}M^{-2}$ complexes were predicted to be unstable with positive $E_{\rm int}$ values (19.4 and 25.2 kcal/mol, respectively) indicating repulsive interactions in these complexes.

Next, modified Henderson-Hasselbalch equations were utilized to determine the mole fractions of the neutral and deprotonated forms of the surface and the adhesive molecule based on their corresponding p K_a values (Figure S20).⁴² The derived mole fraction values were then used to determine their pH dependency and combined binding energy (E_B) at a given pH (Figure 8). At low pH values (pH < 6), the interaction between SHAM and the surface was dominated by the S⁰M⁰ pair. At intermediate pH values (6 < pH < 10), the interaction was dominated by S⁻¹M⁻¹ with small contributions from S⁰M⁻¹ and S⁻¹M⁰ pairs. This is not the case with higher pH values (pH > 10), for which the repulsive $S^{-1}M^{-2}$ pairs dominate the interaction between SHAM and the surface. Catechol also demonstrated a similar trend where S⁰M⁰, S⁻¹M⁰, and S⁻¹M⁻¹ dominated at low, intermediate, and elevated pH levels, respectively (Figure S21).

Figure 8c shows the variation in E_B with pH values obtained from the individual pair of the complex at different deprotonation states. At lower pH, a large negative value of $E_{\rm B} = -25$ kcal/mol indicated a strong adhesion of SHAM to the surface. In contrast, a positive $E_{\rm B}$ value at the higher pH affirms the lack of adhesion of SHAM with the surface. A similar pH dependency of $E_{\rm B}$ was observed for catechol interacting with the Si surface. However, a weaker adhesion with $E_{\rm B}=-13~{\rm kcal/mol}$ was observed at acidic pH values. Overall, the experimental results based on JKR contact mechanics testing (Figure 5) are consistent with DFT predictions. Both SHAM- and catechol-based adhesives demonstrated the highest level of adhesion at pH 5, and their adhesive properties decreased with increasing pH. Moreover, SHAM demonstrated stronger adhesion to the Si surface when compared to catechol.

Taken together, SHAM demonstrated the ability to function as a switchable adhesive molecule that could bind to various types of surfaces under wet conditions. SHAM possesses adhesive property that rivaled catechol. The structural similarity between SHAM and catechol likely contributed to the versatility of SHAM in binding to substrates ranging from glass and metal to a polymer surface. Although the adsorption of SHAM onto mineral surfaces has been previously reported, 52,53 the formulation of SHAM into an adhesive have not been previously demonstrated. Most importantly, our report is the first to directly compare the interfacial bonding behavior of SHAM with that of catechol, a well-characterized underwater adhesive moiety. Additionally, SHAM exhibited superior resistant to base treatment. The propensity for catechol to oxidize irreversibly greatly increases the difficulty when fabricating and delivering catechol-containing adhesive.

Currently, there is a limited number of adhesive molecules that can function as underwater switchable adhesives for binding to multiple surface types. Adhesive molecules that rely on electrostatic or supramolecular interactions can only bind to surfaces with a specific chemistry.^{2,3} Catechol remains one of the most versatile adhesive moieties for switchable, wet adhesion. However, a temporary protecting group in the form of boronic acid is required to preserve the reversibility of catechol and it is often difficult to completely dissociate the catechol—boronate complex to fully recover the initial adhesive property of catechol.^{22,23} In contrast, SHAM demonstrated the reversibility needed for switchable adhesion without the need of a protecting group. The use of a single molecule makes SHAM an attractive option in designing switchable adhesives.

4. CONCLUSIONS

SHAM-containing adhesive demonstrated strong interfacial bonding characteristics to different wet surfaces, and the measured adhesive properties of SHAM were comparable to those of catechol. Additionally, the adhesive property of SHAM decreased with increasing pH levels. When SHAM was exposed to acidic pH, it fully recovered its initial adhesive property. This is drastically different from the catechol-containing adhesive, which did not recover its adhesive property due to irreversible oxidation. The DFT results find a proton-sharing mediated interaction between the O atom of the deprotonated SHAM and the H atom of the surface. Additionally, DFT calculations confirmed the experimental results where SHAM exhibited pH-dependent surface bonding behavior. The findings reported here demonstrated that

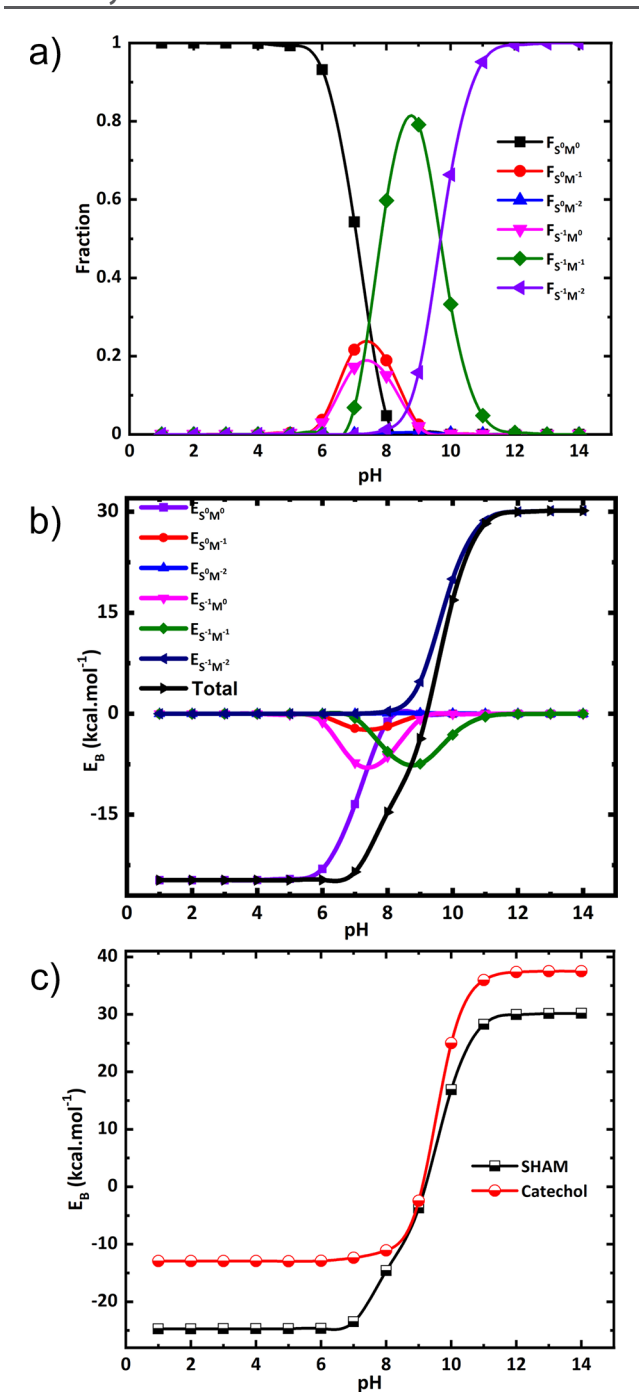


Figure 8. pH-dependent (a) mole fractions and (b) binding energies of various combinations of SHAM and Si at different protonation states. (c) Total binding energy $(E_{\rm B})$ for SHAM and catechol interacting with the Si surface at varying pH levels.

SHAM can function as a pH-responsive and switchable adhesive molecule for binding to different wet surfaces.

ASSOCIATED CONTENT

Supporting Information

The Supporting Information is available free of charge at https://pubs.acs.org/doi/10.1021/acs.chemmater.3c00508.

NMR spectra and standard curves for DHMAAB; FTIR spectra; representative contact curves and $F_{\rm max}$ of SHAM- and catechol-based adhesive influenced by different contact curves or pH levels; $G_{\rm c}$ and $F_{\rm max}$ of

SHAM-based adhesive influences by different indentor speed or interfacial liquid levels; the energy vs distance curves for different molecular contacting orientations; and the mole fractions and interaction between different combinations of neutral and deprotonated states of silica and SHAM and catechol (PDF)

AUTHOR INFORMATION

Corresponding Author

Bruce P. Lee — Biomedical Engineering Department, Michigan Technological University, Houghton, Michigan 49931, United States; orcid.org/0000-0002-6529-0032; Email: bplee@mtu.edu

Authors

Kan Wang — Biomedical Engineering Department, Michigan Technological University, Houghton, Michigan 49931, United States

Lokanath Patra — Physics Department, Michigan Technological University, Houghton, Michigan 49931, United States; Oorcid.org/0000-0002-1050-5665

Bo Liu – Biomedical Engineering Department, Michigan Technological University, Houghton, Michigan 49931, United States

Zhongtian Zhang – Biomedical Engineering Department, Michigan Technological University, Houghton, Michigan 49931, United States

Ravindra Pandey — Physics Department, Michigan Technological University, Houghton, Michigan 49931, United States; oorcid.org/0000-0002-2126-1985

Complete contact information is available at: https://pubs.acs.org/10.1021/acs.chemmater.3c00508

Author Contributions

K.W. led data curation, formal analysis, and writing of the original draft. L.P. supported data curation, formal analysis, and writing of the original draft associated with DFT analysis. B.L. and Z.Z. supported data curation. R.P. and B.P.L. contributed to project supervision. B.P.L. led funding acquisition and project administration. All authors contributed to editing the manuscript.

Funding

This project was funded by the Office of Naval Research under award number N00014-20-1-2230, the National Science Foundation under award number CMMI 2119019, and the National Institutes of Health under award number R15GM135875.

Notes

The authors declare no competing financial interest.

ACKNOWLEDGMENTS

The authors thank Late Prof. Max Seel for fruitful discussions. Computational resources at Michigan Technological University with the SUPERIOR high-performance computing cluster were utilized.

ABBREVIATIONS

SHAM, salicylhydroxamic acid; MFPs, mussel foot proteins; DOPA, 3,4-dihydroxyphenylalanine; DHMAAB, *N*,2-dihydroxy-4-methacrylamidobenzamide; JKR, Johnson–Kendall–Roberts; DFT, density functional theory; ADHB, 4-amino-*N*,2-dihydroxybenzamide; THF, tetrahydrofuran; PBS, phosphate-

buffered saline; HCl, hydrochloric acid; NaOH, sodium hydroxide; NaCl, sodium chloride; DMSO, dimethyl sulfoxide; MEA, methoxyethyl methacrylate; TMSPMA, 3-(trimethoxysilyl)propyl methacrylate; MACl, mechacryloyl chloride; DMPA, 2,2-dimethoxy-2-phenylacetophenone; MBAA, methylene-bis-acrylamide; PTFE, polytetrafluoroethylene; DMA, dopamine methacrylamide; NMR, nuclear magnetic resonance; VASP, vienna ab-initio simulation package; PAW, projected augmented wave; SiOH, silanols; $E_{\rm int}$ interaction energy; FTIR, Fourier transform infrared; $W_{\rm adh}$, work of adhesion; $S_{\rm adh}$, adhesion strength

REFERENCES

- (1) Croll, A. B.; Hosseini, N.; Bartlett, M. D. Switchable adhesives for multifunctional interfaces. *Adv. Mater. Technol.* **2019**, 4, No. 1900193.
- (2) Liu, Z.; Yan, F. Switchable Adhesion: On-Demand Bonding and Debonding. *Adv. Sci.* **2022**, *9*, No. 2200264.
- (3) Fan, H.; Gong, J. P. Bioinspired underwater adhesives. *Adv. Mater.* **2021**, 33, No. 2102983.
- (4) Lee, H.; Um, D. S.; Lee, Y.; Lim, S.; Kim, H. J.; Ko, H. Octopus-inspired smart adhesive pads for transfer printing of semiconducting nanomembranes. *Adv. Mater.* **2016**, *28*, 7457–7465.
- (5) Hwang, I.; Kim, H. N.; Seong, M.; Lee, S. H.; Kang, M.; Yi, H.; Bae, W. G.; Kwak, M. K.; Jeong, H. E. Multifunctional smart skin adhesive patches for advanced health care. *Adv. Healthcare Mater.* **2018**, 7, No. 1800275.
- (6) Wang, S.; Luo, H.; Linghu, C.; Song, J. Elastic Energy Storage Enabled Magnetically Actuated, Octopus-Inspired Smart Adhesive. *Adv. Funct. Mater.* **2021**, *31*, No. 2009217.
- (7) Zhang, Y.; Ma, S.; Li, B.; Yu, B.; Lee, H.; Cai, M.; Gorb, S. N.; Zhou, F.; Liu, W. Gecko's feet-inspired self-peeling switchable dry/wet adhesive. *Chem. Mater.* **2021**, *33*, 2785–2795.
- (8) Xu, K.; Zi, P.; Ding, X. Learning from biological attachment devices: applications of bioinspired reversible adhesive methods in robotics. *Front. Mech. Eng.* **2022**, *17*, 43.
- (9) Northen, M. T.; Greiner, C.; Arzt, E.; Turner, K. L. A Gecko-inspired reversible adhesive. *Adv. Mater.* **2008**, *20*, 3905–3909.
- (10) Sudre, G.; Olanier, L.; Tran, Y.; Hourdet, D.; Creton, C. Reversible adhesion between a hydrogel and a polymer brush. *Soft Matter* **2012**, *8*, 8184–8193.
- (11) Zhou, Y.; Chen, M.; Ban, Q.; Zhang, Z.; Shuang, S.; Koynov, K.; Butt, H.-J. R.; Kong, J.; Wu, S. Light-switchable polymer adhesive based on photoinduced reversible solid-to-liquid transitions. *ACS Macro Lett.* **2019**, *8*, 968–972.
- (12) Del Grosso, C. A.; Leng, C.; Zhang, K.; Hung, H.-C.; Jiang, S.; Chen, Z.; Wilker, J. J. Surface hydration for antifouling and bioadhesion. *Chem. Sci.* **2020**, *11*, 10367–10377.
- (13) Waite, J. H.; Harrington, M. J. Following the thread: Mytilus mussel byssus as an inspired multi-functional biomaterial. *Can. J. Chem.* **2022**, *100*, 197–211.
- (14) Lee, H.; Lee, B. P.; Messersmith, P. B. A reversible wet/dry adhesive inspired by mussels and geckos. *Nature* **2007**, *448*, 338–341.
- (15) Saiz-Poseu, J.; Mancebo-Aracil, J.; Nador, F.; Busqué, F.; Ruiz-Molina, D. The chemistry behind catechol-based adhesion. *Angew. Chem., Int. Ed.* **2019**, *58*, 696–714.
- (16) Pinnataip, R.; Lee, B. P. Oxidation Chemistry of Catechol Utilized in Designing Stimuli-Responsive Adhesives and Antipathogenic Biomaterials. ACS Omega 2021, 6, 5113–5118.
- (17) Zhang, W.; Wang, R.; Sun, Z.; Zhu, X.; Zhao, Q.; Zhang, T.; Cholewinski, A.; Yang, F. K.; Zhao, B.; Pinnaratip, R.; Forooshani, P. K.; Lee, B. P. Catechol-functionalized hydrogels: biomimetic design, adhesion mechanism, and biomedical applications. *Chem. Soc. Rev.* 2020, 49, 433–464.
- (18) Lee, H. A.; Park, E.; Lee, H. Polydopamine and its derivative surface chemistry in material science: a focused review for studies at KAIST. *Adv. Mater.* **2020**, *32*, No. 1907505.

- (19) Park, H. K.; Park, J. H.; Lee, H.; Hong, S. Material-Selective Polydopamine Coating in Dimethyl Sulfoxide. *ACS Appl. Mater. Interfaces* **2020**, *12*, 49146–49154.
- (20) Park, E.; Ryu, J. H.; Lee, D.; Lee, H. Freeze—Thawing-Induced Macroporous Catechol Hydrogels with Shape Recovery and Spongelike Properties. *ACS Biomater. Sci. Eng.* **2021**, *7*, 4318–4329.
- (21) Narkar, A. R.; Kelley, J. D.; Pinnaratip, R.; Lee, B. P. Effect of Ionic Functional Groups on the Oxidation State and Interfacial Binding Property of Catechol-Based Adhesive. *Biomacromolecules* **2018**, *19*, 1416–1424.
- (22) Narkar, A. R.; Barker, B.; Clisch, M.; Jiang, J.; Lee, B. P. pH Responsive and Oxidation Resistant Wet Adhesive based on Reversible Catechol-Boronate Complexation. *Chem. Mater.* **2016**, 28, 5432–5439.
- (23) Liu, B.; Li, J.; Zhang, Z.; Roland, J. D.; Lee, B. P. pH responsive antibacterial hydrogel utilizing catechol—boronate complexation chemistry. *Chem. Eng. J.* **2022**, *441*, No. 135808.
- (24) Pillai, K.; Costello, B.; Oresajo, C.; Ceccoli, J. Cosmetic compositions containing combinations of hydroxamate derivatives and antioxidants in a liposomal delivery system. Google Patents US20060165641A1, 2006.
- (25) Urbański, T. Salicylhydroxamic acid as an antitubercular agent. *Nature* **1950**, *166*, 267–268.
- (26) Hassan, S. S.; El-Bahnasawy, R. M.; Rizk, N. M. Potentiometric determination of salicylhydroxamic acid (urinary struvite stone inhibitor) based on the inhibition of urease activity. *Anal. Chim. Acta* **1997**, *351*, 91–96.
- (27) Kane, S. N.; Gupta, A.; Ali, S. M.; Khadikar, P. V. Mössbauer study of some metal chelates of salicylhydroxamic acid and benzohydroxamic acid. *Hyperfine Interact.* **1987**, *35*, 927–930. WorldCat.org
- (28) Al Azzam, K. M.; El Kassed, W. New, simple, sensitive and validated spectrophotometric method for the determination of salicylhydroxamic acid in capsules and raw material according to the ICH guidelines. *Egypt. J. Basic Appl. Sci.* **2017**, *4*, 345–349.
- (29) Glorius, M.; Moll, H.; Geipel, G.; Bernhard, G. Complexation of uranium (VI) with aromatic acids such as hydroxamic and benzoic acid investigated by TRLFS. *J. Radioanal. Nucl. Chem.* **2008**, 277, 371–377.
- (30) Bhuiyan, M. S. A.; Roland, J. D.; Liu, B.; Reaume, M.; Zhang, Z.; Kelley, J. D.; Lee, B. P. In Situ Deactivation of Catechol-Containing Adhesive Using Electrochemistry. *J. Am. Chem. Soc.* **2020**, *142*, 4631–4638.
- (31) Narkar, A. R.; Kendrick, C.; Bellur, K.; Leftwich, T.; Zhang, Z.; Lee, B. P. Rapidly responsive smart adhesive-coated micropillars utilizing catechol-boronate complexation chemistry. *Soft Matter* **2019**, 15, 5474–5482.
- (32) Bhuiyan, M. S. A.; Liu, B.; Manuel, J.; Zhao, B.; Lee, B. P. Effect of Conductivity on In Situ Deactivation of Catechol—Boronate Complexation-Based Reversible Smart Adhesive. *Biomacromolecules* **2021**, 22, 4004–4015.
- (33) Ciavarella, M.; Joe, J.; Papangelo, A.; Barber, J. The role of adhesion in contact mechanics. *J. R. Soc., Interface* **2019**, *16*, No. 20180738.
- (34) Shull, K. R. Contact mechanics and the adhesion of soft solids. *Mater. Sci. Eng.*, R **2002**, *36*, 1–45.
- (35) Choi, S. T. Extended JKR theory on adhesive contact of a spherical tip onto a film on a substrate. *J. Mater. Res.* **2012**, 27, 113–120.
- (36) Kresse, G.; Furthmüller, J. Efficient iterative schemes for ab initio total-energy calculations using a plane-wave basis set. *Phys. Rev. B* **1996**, *54*, 11169.
- (37) Blöchl, P. E. Projector augmented-wave method. *Phys. Rev. B* **1994**, *50*, 17953.
- (38) Perdew, J. P.; Burke, K.; Ernzerhof, M. Generalized gradient approximation made simple. *Phys. Rev. Lett.* **1996**, *77*, 3865.
- (39) Monkhorst, H. J.; Pack, J. D. Special points for Brillouin-zone integrations. *Phys. Rev. B* **1976**, *13*, 5188.

Chemistry of Materials Article pubs.acs.org/cm

- (40) Mian, S. A.; Saha, L. C.; Jang, J.; Wang, L.; Gao, X.; Nagase, S. Density functional theory study of catechol adhesion on silica surfaces. J. Phys. Chem. C 2010, 114, 20793-20800.
- (41) Pluth, J.; Smith, J.; Faber, J., Jr. Crystal structure of low cristobalite at 10, 293, and 473 K: Variation of framework geometry with temperature. J. Appl. Phys. 1985, 57, 1045-1049.
- (42) Ahmed, K.; Inamdar, S. N.; Rohman, N.; Skelton, A. A. Acidity constant and DFT-based modelling of pH-responsive alendronate loading and releasing on propylamine-modified silica surface. Phys. Chem. Chem. Phys. 2021, 23, 2015-2024.
- (43) Hu, C.; Yu, L.; Zheng, Z.; Wang, J.; Liu, Y.; Jiang, Y.; Tong, G.; Zhou, Y.; Wang, X. Tannin as a gatekeeper of pH-responsive mesoporous silica nanoparticles for drug delivery. RSC Adv. 2015, 5, 85436-85441.
- (44) Ong, S.; Zhao, X.; Eisenthal, K. B. Polarization of water molecules at a charged interface: second harmonic studies of the silica/water interface. Chem. Phys. Lett. 1992, 191, 327-335.
- (45) Hiemstra, T.; Van Riemsdijk, W. H.; Bolt, G. Multisite proton adsorption modeling at the solid/solution interface of (hydr) oxides: A new approach: I. Model description and evaluation of intrinsic reaction constants. J. Colloid Interface Sci. 1989, 133, 91-104.
- (46) Fan, H.; Wang, J.; Zhang, Q.; Jin, Z. Tannic acid-based multifunctional hydrogels with facile adjustable adhesion and cohesion contributed by polyphenol supramolecular chemistry. ACS Omega 2017, 2, 6668-6676.
- (47) Mathis, C. H.; Spencer, N. D. A two-step method for ratedependent nano-indentation of hydrogels. Polymer 2018, 137, 276-
- (48) Efremov, Y. M.; Bagrov, D.; Kirpichnikov, M.; Shaitan, K. Application of the Johnson-Kendall-Roberts model in AFM-based mechanical measurements on cells and gel. Colloids Surf., B 2015, 134,
- (49) Payam, A. F. Modeling and Analysis of the Capillary Force for Interactions of Different Tip/Substrate in AFM Based on the Energy Method. ACS Meas. Sci. Au 2023, 3, 194-199.
- (50) Henkelman, G.; Arnaldsson, A.; Jónsson, H. A fast and robust algorithm for Bader decomposition of charge density. Comput. Mater. Sci. 2006, 36, 354-360.
- (51) Inamdar, S. N.; Ahmed, K.; Rohman, N.; Skelton, A. A. Novel pKa/DFT-Based Theoretical Model for Predicting the Drug Loading and Release of a pH-Responsive Drug Delivery System. J. Phys. Chem. C 2018, 122, 12279-12290.
- (52) Cao, S.; Cao, Y.; Liao, Y.; Ma, Z. Depression Mechanism of Strontium Ions in Bastnaesite Flotation with Salicylhydroxamic Acid as Collector. Minerals 2018, 8, 66.
- (53) Miao, Y.; Wen, S.; Zuo, Q.; Shen, Z.; Zhang, Q.; Feng, Q. Coadsorption of NaOL/SHA composite collectors on cassiterite surfaces and its effect on surface hydrophobicity and floatability. Sep. Purif. Technol. 2023, 308, No. 122954.
- (54) Heo, J.; Kang, T.; Jang, S. G.; Hwang, D. S.; Spruell, J. M.; Killops, K. L.; Waite, J. H.; Hawker, C. J. Improved performance of protected catecholic polysiloxanes for bioinspired wet adhesion to surface oxides. J. Am. Chem. Soc. 2012, 134, 20139-20145.

□ Recommended by ACS

Electrochemical Deactivation of Switchable Catechol-Containing Smart Adhesive from Nonconductive Surfaces

Md Saleh Akram Bhuiyan, Bruce P. Lee, et al.

MAY 17 2023

ACS APPLIED POLYMER MATERIALS

READ 2

Engineering of Adhesion at Metal-Poly(lactic acid) Interfaces by Poly(dopamine): The Effect of the Annealing **Temperature**

Georgios Kafkopoulos, G. Julius Vancso, et al.

JULY 06, 2023

ACS APPLIED POLYMER MATERIALS

READ **C**

Multifunctional Platform for Covalent Titanium Coatings: Micro-FTIR, XPS, and NEXAFS Characterizations

Martina Marsotto, Monica Orsini, et al.

MAY 02, 2023

LANGMUIR

RFAD 17

Robust Electrostatically Interactive Hydrogel Coatings for Macroscopic Supramolecular Assembly via Rapid Wet Adhesion

Yijing Liu, Mengjiao Cheng, et al.

APRIL 19, 2023

ACS APPLIED MATERIALS & INTERFACES

RFAD 🗹

Get More Suggestions >